Structure and Properties of an Amorphous Metal Organic Framework

SUPPLEMENTARY INFORMATION

Thomas D. Bennett,[1] Andrew L. Goodwin,[2] Martin T. Dove,[2]
David A. Keen,[3,4] Matthew G. Tucker,[3] Emma R. Barney,[3] Alan K. Soper,[3]
Erica G. Bithell,[1] Jin-Chong Tan,[1] Anthony K. Cheetham[1*]

[1]Department of Materials Science and Metallurgy, University of Cambridge, Cambridge CB2 3QZ, U.K.

[2]Department of Earth Sciences, University of Cambridge, Downing Street, Cambridge CB2 3EQ, U.K.

[3]ISIS Facility, Rutherford Appleton Laboratory, Harwell Science and Innovation Campus, Didcot, Oxfordshire OX11 0QX, U.K.

[4]Department of Physics, Oxford University, Clarendon Laboratory, Parks Road, Oxford OX1 3PU, U.K.

[*]To whom correspondence should be addressed; E-mail: akc30@cam.ac.uk.

Contents

1 Synthesis

(ZIF-4): Zn(im-d_3)$_2$·(DMF-d_7) A solid mixture of zinc nitrate hexadeuterate Zn(NO_3)·6D_2O (0.12 g, 3.88×10^{-4} mol), itself prepared by repeated dissolution and recrystallisation of zinc nitrate hexahydrate ($\geq$99%, Aldrich) in D_2O (99.98% deuteration, Aldrich), and deuterated imidazole (D-(im-d_3)) (0.09 g, 1.25×10^{-3} mol; Cambridge Isotopes, 98% deuteration) was dissolved in 5 ml dimethylformamide (DMF) in a 23 ml teflon-lined autoclave. The mixture was heated in a programmable oven at a rate of 2 °C min^{-1} to 130 °C, then kept at this temperature for 48 h and cooled at a rate of 0.5 °C min^{-1} to room temperature. Colourless rhombohedral crystals of ZIF-4 were filtered from the mother liquor, before being washed with dichloromethane (5 ml $\times$ 2) and dried in air (30 min).

This procedure was repeated 35 times, the products of each reaction combined, and the total quantity of product immersed in DMF-d_7 (10 ml; Cambridge Isotopes, 99.5% deuteration) for 48 h to allow exchange between the hydrogenous included DMF and the deuterated solvent. The crystals were subsequently filtered and air-dried (30 min) to afford 3.024 g of deuterated ZIF-4. The level of deuteration was assessed from the incoherent scattering intensity in neutron diffraction experiments: it was found that DMF exchange had not been complete, but that the zinc imidazolate framework was deuterated to within normal tolerances (*i.e.* to the expected level of 98%).

(ZIF-zni): Zn(im)$_2$ An aqueous solution (2 ml) of zinc nitrate hexahydrate Zn(NO_3)$_2$·6H_2O (0.20 M, 4×10^{-3} mol) was combined with sodium boron imidazolate NaB(im)$_4$ (0.12 g, 4×10^{-3} mol) and DMF (5 ml). The resultant solution was placed in a 23 ml Teflon-lined autoclave and heated to 180 °C for 72 h in a programmable oven, before cooling to room temperature at a rate of 5 °C. Rod shaped single crystals were isolated from the mother liquor by filtration, washed with dichloromethane (5 ml $\times$ 2) and air-dried.

2 Thermogravimetric analysis

Thermogravimetric analysis (TGA) was performed using a TA instruments Q-500 series thermal gravimetric analyser, with the sample ($\sim$20 mg) held on a platinum pan under a continuous flow of dry N_2 gas. The TGA curve in Fig. S1 was obtained using a heating rate of 10 °C min^{-1}. Two primary weight-loss stages were observed. The first, at around 200 °C, corresponds to loss

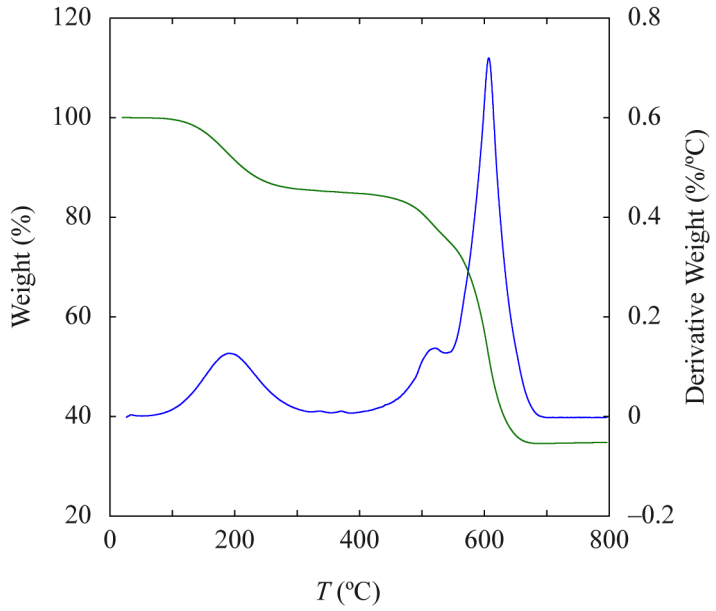

Figure S1: The TGA trace (green) and its derivative (blue) of deuterated $Zn(im)_2 \cdot DMF$.

of all 0.56 molar equivalents of DMF. The second coincides with framework decomposition, which can be seen to occur at around 500 °C. There is no mass loss associated with the amorphization process at 300 °C.

3 Neutron Total Scattering

Neutron total scattering data from $Zn(im)_2$ were measured on the neutron time-of-flight diffractometer GEM at ISIS.[S1] A finely-powdered sample of perdeuterated solvated ZIF-4 was placed inside a cylindrical thin-walled vanadium can of ∼60 mm length and 8 mm diameter and mounted inside a furnace with vanadium heating element and heat shields. Data were collected from the as-prepared sample at room temperature, at 205 °C, which coincided with complete removal of DMF, and at 300 °C when the diffraction pattern showed that the sample was completely amorphous. The sample was then cooled to room temperature and a further data set was collected from the recovered amorphous sample. After removing a small quantity of sample to measure the X-ray total scattering pattern, the sample was re-heated into the ZIF-zni phase and total scattering data were collected at 400 °C. Additional measurements of the scattering

from an 8 mm vanadium rod, the empty instrument, empty furnace and empty 8 mm vanadium can inside the furnace were made for background subtraction and to place the scattering data on an absolute scale. The data were corrected using the Gudrun software, based on the Atlas routines[S2] which also merges the data from different detector banks into a single normalised total scattering structure factor, $S(Q)$.[S3]

4 X-ray Total Scattering

X-ray total scattering data were collected at room temperature from recovered a-ZIF and ZIF-zni samples using a PANalytical Ag-source X'Pert Pro MPD lab diffractometer which is capable of measuring data between $\sim$0.5$<$ Q $<\sim$22 Å^{-1}. The finely-powdered samples (identically those used in the neutron scattering experiments) were carefully loaded into 0.5 mm diameter silica capillaries and mounted onto the rotating sample stage of the diffractometer. Data from an empty silica capillary were also collected using the same diffractometer settings for background subtraction. Data collection times were typically $\sim$18 hours. Corrections for background, multiple scattering, container scattering, Compton scattering, absorption and Bremsstrahlung effects were applied using the GudrunX program.[S4] The corrected data were placed on an absolute scale using a procedure derived from the Krogh-Moe method[S5] which uses a single-atom scattering sharpening factor to emphasise scattering amplitudes for increasing Q.[S6]

Comparisons of the normalised reciprocal space data for a-ZIF and ZIF-zni and the corresponding Fourier transforms are given in Fig. S2. Again, the local structure is very similar in the two materials, but there is a fundamental difference in the long-range structural correlations. We also note that the increased relative scattering power of Zn atoms in these X-ray data compared to the neutron total scattering data allows one to observe clearly the Zn...Zn peak at *ca* 6 Å in the $D(r)$ function. It is only at larger distances that one observes any meaningful difference in the pair distribution functions.

5 GSAS Refinements

Verification of the phases identified as ZIF-4 and ZIF-zni was achieved via Rietveld analysis of the neutron powder diffraction patterns obtained as described above, performed using

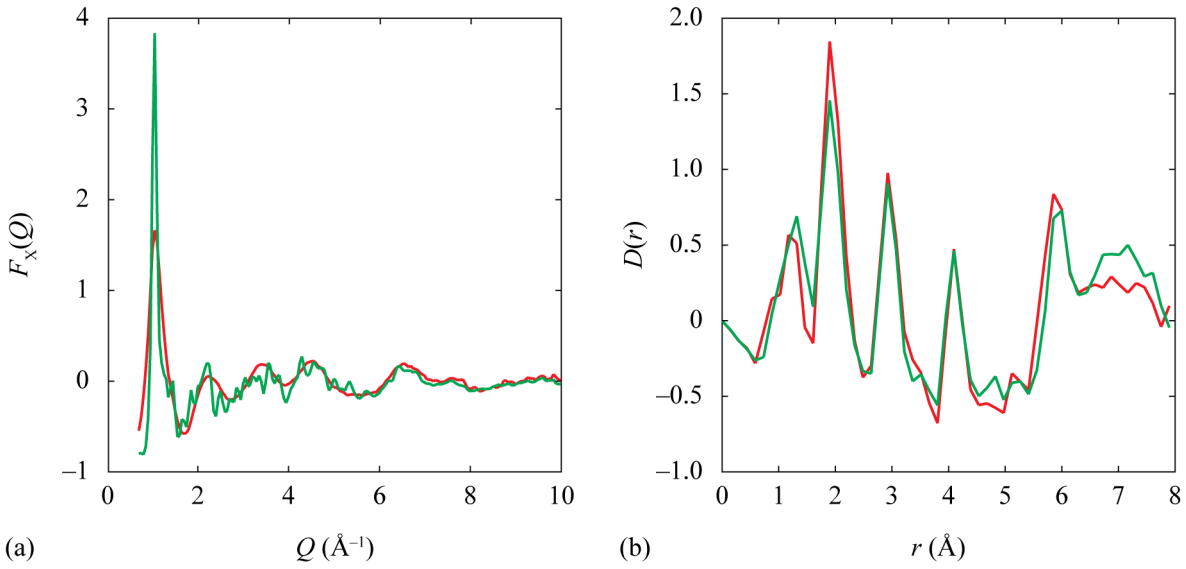

Figure S2: X-ray total scattering data measured for the identical samples described in the main text. (a) Low-Q region of the X-ray total scattering function $F_{\mathrm{X}}(Q)$ for a-ZIF (red) and ZIF-zni (green); (b) Low-r region of the effective differential pair correlation function $D(r)$ calculated via Fourier transform of $F_{\mathrm{X}}(Q)$ up to $Q_{\mathrm{max}} = 20\,\text{Å}^{-1}$. Despite the fundamental differences in long-range correlations evident in (a), the two materials have indistinguishable local structures.

the program GSAS.[S7] The previously-published crystal structures were used as starting models.[S8,S9] Due to the large number of refinable variables, rigid body constraints were applied to the imidazole groups, together with Zn–N bond distance restraints. The fits obtained are shown in Fig. S3; these confirm the nature of the phases and also that the ZIF-4 phase is indeed desolvated at 300 °C, prior to its transformation to a-ZIF. Key crystallographic data and refinement statistics are given in Table S1; atomic coordinates are similar to those published elsewhere.[S8,S9]

6 Reverse Monte Carlo Modelling

The program RMCProfile[S10] was used to refine atomistic models against the neutron $F(Q)$ and $G(r)$ data and X-ray $F(Q)$ data collected for a-ZIF at 320 °C as described above. The following three different starting models were used, each of which contained 512 formula units of $Zn(im)_2$

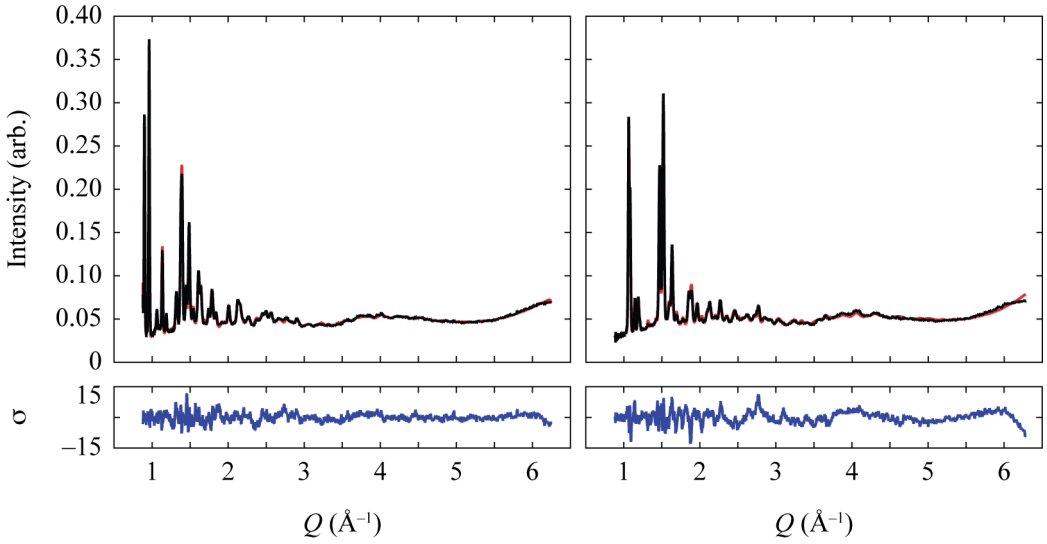

Figure S3: GSAS fits (red lines) to neutron diffraction patterns (black lines), together with relative difference functions σ = (fit-data)/error for desolvated ZIF-4 (left) and ZIF-zni (right).

Table S1: Crystallographic details of the structural model refined using GSAS against the neutron scattering data shown in Fig. S3.

Phase	**ZIF-4**	**ZIF-zni**
Formula	$ZnC_6D_6N_4$	$ZnC_6D_6N_4$
T/K	573	673
Crystal system	Orthorhombic	Tetragonal
Space group	$Pbca$	$I4_1cd$
a/Å	15.5571(10)	23.6039(8)
b/Å	15.6940(8)	23.6039(8)
c/Å	18.0357(14)	12.3683(7)
V/Å^3	4403.47(29)	6890.9(5)
Z	16	32
Fitted R_p	0.0332	0.0415

(= 8,704 atoms) within a box approximately 50 Å in each linear dimension and a number density of 0.0693 $Å^{-3}$.[S11]

1. *ZIF-4 model:* The RMC box axes were related to the $Pbca$ unit cell[S8] via the transformation:

$$\begin{bmatrix} \mathbf{a} \\ \mathbf{b} \\ \mathbf{c} \end{bmatrix}_{\text{RMC}} = \begin{bmatrix} -2 & 0 & 2 \\ 2 & 0 & 2 \\ 0 & 4 & 0 \end{bmatrix} \begin{bmatrix} \mathbf{a} \\ \mathbf{b} \\ \mathbf{c} \end{bmatrix}_{Pbca}$$

2. *ZIF-zni model:* The RMC box corresponded to a 2 × 2 × 4 supercell of the $I4_1cd$ unit cell.[S9]

3. *a-SiO_2 model:* The RMC box measured 50.08 Å × 50.08 Å × 50.08 Å, and was based on a continuous random network model of a-SiO_2 that itself contained 512 Si atoms and 1024 O atoms. Zn atoms were placed on Si sites and imidazolate molecules placed on O site. Further details are given below.

Models 1 and 2 were refined in duplicate using two slightly different box dimensions: in one set the RMC box had the same isotropic dimensions as the a-SiO_2 model, and in the other an anisotropic box size of 47.36 Å × 47.36 Å × 56.00 Å was used (the aspect ratio here taken from the ZIF-zni $I4_1cd$ cell[S9]); in practice there was no significant difference in the quality of the fits obtained.

In all cases, the same set of constraints/restraints were applied: connectivity constraints preserved the underlying network structure; molecular geometry restraints encouraged reasonable imidazolate ring geometries; N–Zn–N bond angle restraints ensured near-tetrahedral Zn coordination. Identical refinement strategies yielded the fits shown in Fig. S4, which clearly show that the a-SiO_2 model best captures the fundamental structure of a-ZIF.

Creating the continuous random network

The starting point for the continuous random network model of a-ZIF was a model of amorphous silica, that had in turn been derived from a CRN model of amorphous silicon constructed using the Wooten–Winer–Weaire ("WWW") method.[S12] The amorphous silica model

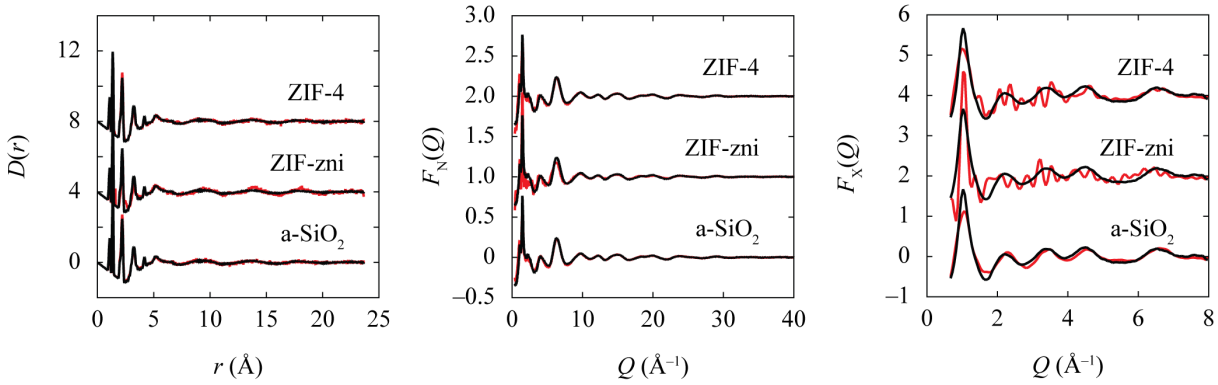

Figure S4: RMC fits (red lines) to experimental total scattering data (black lines), calculated for equilibrium configurations for models based on the ZIF-4 (top), ZIF-zni (middle) and a-SiO_2 (bottom) topologies. Curves have been raised by appropriate constant values for clarity.

was built by expanding the silicon model, then adding oxygen atoms half-way along each nearest-neighbour Si–Si vector, and finally relaxing the structure by running molecular dynamics simulations.[S13,S14] This relaxed silica model contained bond-angle distributions that are consistent with experiment.[S15] To construct a metal imidazolate framework from an arbitrary parent silica model we developed a general utility program SILICA2ZIF to convert any silica network to the corresponding ZIF structure, aligning the orientation of the imidazolate molecular ligand.[S16] Applying this approach to the WWW-derived a-SiO_2 model described above gave the a-ZIF starting model used in RMC refinement.

7 Nanoindentation Studies

The Young's modulus (E) and hardness (H) of single crystals/monoliths of ZIF-4, a-ZIF and ZIF-zni were determined using an MTS NanoIndenter XP (Agilent Technologies), equipped with a Continuous Stiffness Measurement (CSM) module. All measurements were conducted with a three-sided pyramidal (Berkovich) diamond tip (end radius $\sim$50 nm) under ambient conditions. Thermal drifts were maintained at $<$0.05 nm s^{-1} throughout all experiments.

The crystallographic orientations of untwinned crystals were identified via single-crystal X-ray diffraction. Fig. S5 depicts the typical crystal habits and their low-index planes. Selected crystals/monoliths were cold-mounted using an Epofix resin (Struers Ltd.) and then polished

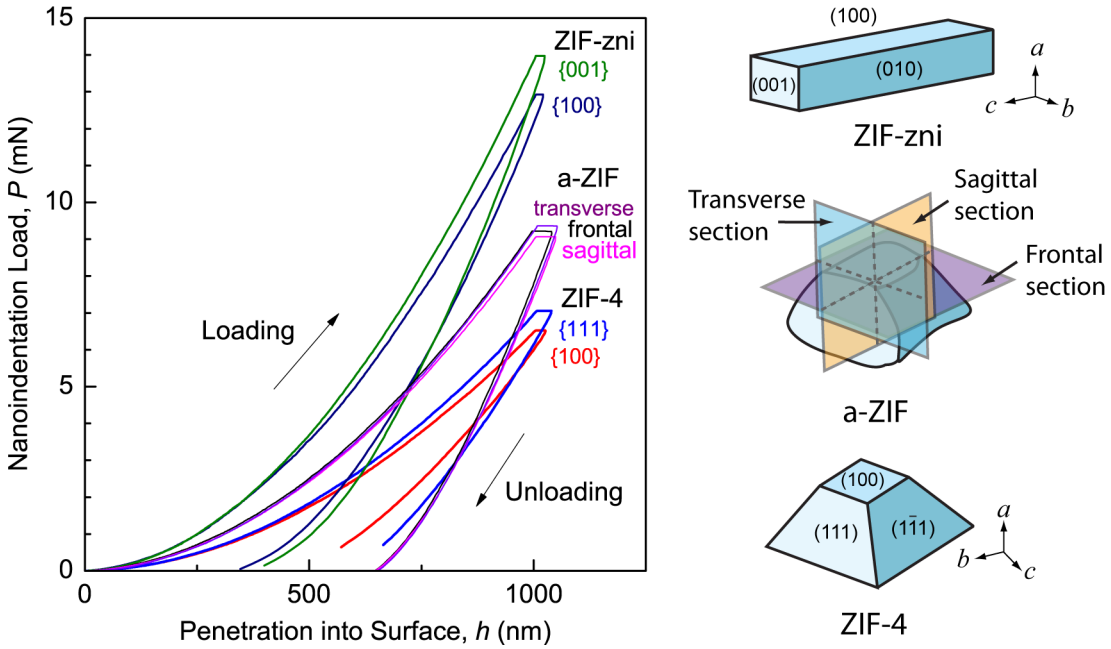

Figure S5: Typical load versus displacement (P-h) curves obtained from dynamic mode (CSM) nanoindentation of different phases, along the chosen orientations. In all cases, the Berkovich indenter axis was oriented at a right angle to the indented facet and the maximum surface penetration depth was set at 1000 nm. Such curves were used to derive elastic modulus (Fig. S7(a)) and hardness information as a function of depth.

using increasingly-fine diamond suspensions to attain a final surface finish of less than 10 nm (rms), as determined from atomic force microscopy (AFM). Such procedures have been successfully employed in preparing other hybrid inorganic-organic single crystals for nanoindentation studies.[S17,S18]

Under the dynamic CSM mode, E and H can be obtained as a function of indentation depth by monitoring the variation in the surface contact stiffness. This was done by superimposing a 2 nm sinusoidal displacement at 45 Hz onto the loading signal. The loading and unloading strain rates were maintained at 50 mHz. At least 20 separate indents were made on each phase and along a predetermined orientation. In addition, to avoid interaction of plastically deformed zones, the inter-indent spacing was at least 30 times the maximum indentation depth (h_{max} =1000 nm).

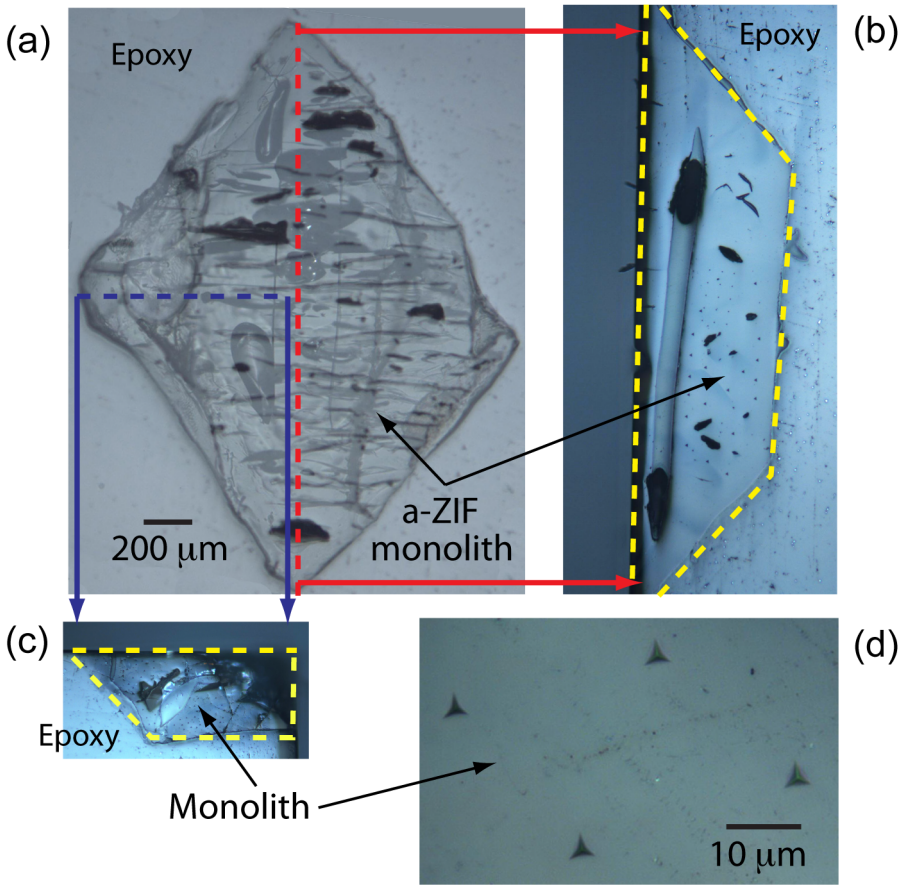

Figure S6: Morphology of the a-ZIF monolith and the 3 orthogonal orientations in which the Young's moduli and hardnesses were determined by means of nanoindentation experiments (Table S2). Note the curved external surfaces, the internal cavities and some visible surface cracks. At least 20 indents were made onto the (a) frontal, (b) sagittal, and (c) transverse cross-sections. It is noted that the frontal section (a), was aligned approximately parallel to the $[100]$ axis of the original ZIF-4 single crystal (see schematic in Fig. S5). In particular, indents were made on carefully selected regions free of (visible) cracks, cavities and surface contamination – see panel (d).

Fig. S6 depicts the geometry of the amorphized a-ZIF monolith and the three orthogonal planes on which indentation was performed. Their mechanical properties together with those of crystalline ZIF-4, ZIF-zni, and a partially-recrystallized a-ZIF/ZIF-zni monolith are summarized in Fig. S7 and Table S2.

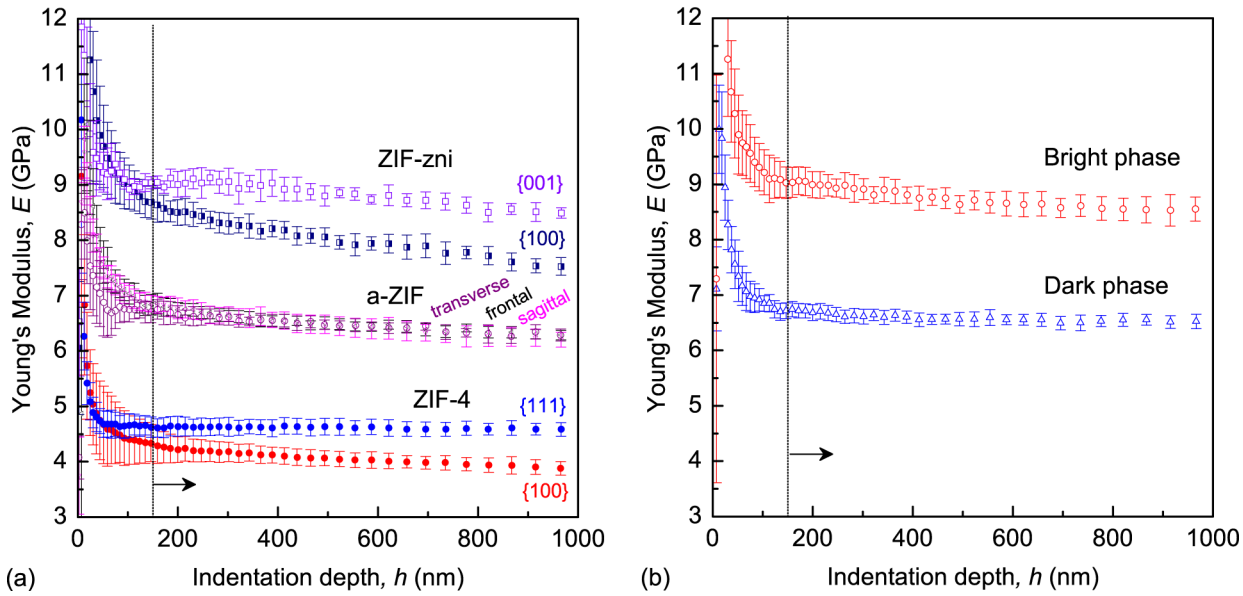

Figure S7: Young's moduli as a function of indentation depth. Error bars give standard deviations calculated from 20 indention experiments. The large scatter over the initial 150 nm is due to imperfect tip-to-sample surface contact; these data were not taken into account when calculating the mean values given in Table S2. Measured moduli were approximately independent of depth for depths greater than ∼150 nm.

Young's moduli (E) were calculated from the measured reduced moduli, E_r, via

$$\frac{1}{E_r} = \left(\frac{1-\nu_s^2}{E}\right) + \left(\frac{1-\nu_i^2}{E_i}\right), \tag{1}$$

where E_i and ν_i are the elastic modulus and Poisson's ratio of the indenter, respectively (for the diamond tip E_i = 1141 GPa and ν_i = 0.07), and ν_s is the sample Poisson's ratio.[S17,S19] All elastic moduli presented here were determined by taking the sample Poisson's ratio to be approximately equal to 0.2, noting that ν_s = 0.18 for a-SiO_2 and 0.3 for MOF-5.[S19,S20] The calculated value of E is in fact not particularly sensitive to the absolute value of ν_s: from Eq. (1) one has that a 50% increase in ν_s from 0.2 to ν_s = 0.3 gives only a 5% difference in the corresponding values of E.

Table S2: Summary of the mechanical properties of ZIF-4, ZIF-zni, a-ZIF and phases derived from a ZIF-4 single crystal that was amorphized and later recrystallized. The moduli and hardnesses tabulated here correspond to the mean values of the CSM data from indentation depths of 150 nm to 1000 nm; standard errors are given in parentheses.

Phase	**Orientation**	**Young's Modulus E (GPa)**	**Hardness H (GPa)**
ZIF-4	$\{111\}$	4.62(13)	0.464(18)
	$\{100\}$	4.08(14)	0.509(29)
ZIF-zni	$\{001\}$	8.88(15)	1.068(21)
	$\{100\}$	8.09(14)	1.090(25)
a-ZIF	Frontal	6.53(6)	0.662(11)
monolith	Sagittal	6.51(14)	0.634(13)
	Transverse	6.50(9)	0.632(14)
Recrystallized	"Bright" phase	8.76(16)	1.16(4)
a-ZIF	"Dark" phase	6.59(8)	0.649(11)

8 Transmission Electron Microscopy

Samples suitable for electron microscopy studies were prepared from ZIF-4 crystals which had been pre-treated to evacuate any residual solvent molecules. These crystals were ground under propan-2-ol to yield fragments a few microns in diameter or smaller, each of which was itself a small single crystal. The resulting suspension was dispersed using an ultrasonic bath, and drops were allowed to evaporate from the surface of standard TEM support films (amorphous holey carbon supported on a copper mesh grid). Transformation between the three phases was achieved by using an *in-situ* heating protocol to replicate the time-periods and temperature values used in the neutron diffraction experiments. The electron diffraction data were collected using a Philips FEI CM30 transmission electron microscope operating at 300 kV, with the beam current reduced to a level where there was minimal perceptible change in the appearance of the diffraction patterns during the exposure time. Diffraction patterns were recorded using

electron imaging plates which were processed using a Ditabis Vario scanner. The contrast of these patterns is low, both because of the low total electron dose and because of the relatively weak scattering from the ZIF phases. For this reason the contrast of all the patterns has been enhanced by fitting a decaying exponential to the background between the peaks/rings and stripping this fitted background from the data.

Note that the pattern reproduced in Fig. 3(h) of the main text is typical of those found after transformation to ZIF-zni, showing diffraction from a number of randomly-overlaid variants within the area defined by the selected area aperture ($\sim$1 μm diameter in the specimen plane). It is occasionally possible to find fragments which have transformed entirely to a single variant. We did not observe any ring patterns such as would be typical of finely-grained polycrystalline material, and for this reason we conclude that the grain size of the ZIF-zni is somewhat smaller than the aperture diameter, but by rather less than an order of magnitude.

9 References

(S1) A. C. Hannon, *Nucl. Instrum. Methods Phys. Res.* A **551**, 88 (2005).

(S2) A. C. Hannon, W. S. Howells, A. K. Soper, *IOP Conf. Ser.* **107**, 193 (1990).

(S3) D. A. Keen, *J. Appl. Cryst.* **34**, 172 (2001).

(S4) A. K. Soper, unpublished.

(S5) J. Krogh-Moe, *Acta Cryst.* **9**, 951 (1956).

(S6) A. K. Soper, *J. Phys.: Cond. Matt.* **19**, 335206 (2007).

(S7) A. C. Larson, R. B. von Dreele, "General structure analysis system (GSAS)," Los Alamos National Laboratory Report No. LAUR 86-748 (2000).

(S8) R. Banerjee, *et al.*, *Science* **319**, 939 (2008).

(S9) R. Lehnert, F. Seel, *Z. Anorg. Allg. Chem.* **464**, 187 (1980).

(S10) M. G. Tucker, D. A. Keen, M. T. Dove, A. L. Goodwin, Q. Hui, *J. Phys.: Cond. Matt.* **19**, 335218 (2007).

(S11) This density gives a volume per formula unit V/Z = 245.28 Å^3 that is equal to the mean of the corresponding crystallographic values for ZIF-4 (V/Z = 275.22 Å^3) and ZIF-zni (V/Z = 215.37 Å^3) at similar temperatures. Pycnometric density measurements confirm that the density of a-ZIF is intermediate to that of the two crystalline phases.

(S12) F. Wooten, K. Winer, D. Weaire, *Phys. Rev. Lett.* **54**, 1392 (1985).

(S13) K. Trachenko, M. T. Dove, K. D. Hammonds, M. J. Harris, V. Heine, *Phys. Rev. Lett.* **81**, 3431 (1998)

(S14) K. O. Trachenko, M. T. Dove, M. J. Harris, V. Heine, *J. Phys.: Condens. Matter* **12**, 8041 (2000).

(S15) M. G. Tucker, D. A. Keen, M. T. Dove, K. Trachenko, *J. Phys.: Condens. Matter* **17**, S67 (2005).

(S16) http://web.me.com/dove_family/martin/codes/silica2zif.html

(S17) J. C. Tan, C. A. Merrill, J. B. Orton, A. K. Cheetham, *Acta Mater.* **57**, 3481 (2009).

(S18) J. C. Tan, J. D. Furman, A. K. Cheetham, *J. Am. Chem. Soc.* **131**, 14252 (2009).

(S19) W. C. Oliver, G. M. Pharr, *J. Mater. Res.* **7**, (1992).

(S20) D. F. Bahr, *et al.*, *Phys. Rev. B* **76**, 184106 (2007).